

**Magnetic composite based on cellulose and GO for latent fingerprint visualization**

Sawsan Dacropy and Samir Kamel

Cellulose and Paper Department, National Research Centre, 33 El Bohouth St., Giza, 12622,

Egypt.

**Abstract**

Magnetite cellulose composite was synthesized from oxidized cellulose, magnetite, and graphene oxide. First, cellulose was oxidized by 2,2,6,6-tetramethylpiperidine-1-oxyl (TEMPO) followed by in situ synthesis of magnetite from $\text{FeSO}_4 \cdot 7\text{H}_2\text{O}$ with FeCl_3 in the presence of TEMPO-oxidized cellulose. Next, graphene oxide (GO) synthesized from graphite by Hummer oxidation method with slight modification was loaded onto magnetite cellulose giving composite utilized for latent fingerprint visualization. The prepared composite was characterized by infrared spectroscopy (FTIR), X-ray diffraction (XRD), thermal gravimetric analysis (TGA), and scanning electron microscope (SEM) techniques. Additionally, the magnetic composite has visualized the latent fingerprints (LFPs) and the cytotoxicity of the prepared composite. Investigating magnetite composite toward normal immortalized skin cells (BJ1) by MTT assay found that the cells treated with composite were affected by 21.3% only. These results show the great application prospects of this eco-friendly powder in criminal investigation and forensic identification.

Keywords: Oxidized Cellulose; Magnetite; Graphene oxide; Cytotoxicity; Latent fingerprint.

1. Introduction

Fingerprints are a characteristic feature of human hands. No two people have the same fingerprint. So, it is a considerable unique approach to biometric identification in forensic science. When fingers touch a surface, residua are transferred to the surface and left a latent fingerprint that cannot be seen by the naked eye[1]. This fingerprint has ridges and grooves that convey individuality and remain unchanged throughout any person's lifetime [2]. Thus, it needs chemical or physical non-toxic material enhancement to make it visible[3]. The common developments strongly depend on using suitable reagents to interact or react easily with the latent fingerprint components as glycerides, fatty acids, and amino acids to enhance the visual contrast against the background surface [4]. Although various methods have been used for latent fingerprint detection, such as vacuum metal deposition[5], scanning Kelvin microprobe[6] and Infrared spectroscopy[7], the powder method is the most common because it is a non-toxic, cost-effective, and simple process. Therefore, fingerprints play a considerable role in many fields such as forensic investigation, safety control, and the medical field[8].

Nanomaterials have a significant impact in recent years due to their remarkable optical, electrical, mechanical, and magnetic properties. Magnetic graphene oxide ($\text{GO}/\text{Fe}_3\text{O}_4$) nanoparticles have many features that encourage researchers to study their applications[8]. Graphene oxide (GO) is a new material with promising properties due to its unique structure. It is composed of a single layer of grapheme that bonds to oxygen in carboxyl, hydroxyl, or epoxy groups. Due to its mechanical, electronic, optical, and thermal properties, GO has a significant role in many applications such as energy storage devices, flexible electronics, sensors, and solar cells[9, 10]. Recently graphene oxide was utilized in latent fingerprints application[4, 8].

Moreover, cellulose is an abundant renewable material, non-toxic, biodegradable, and biocompatible polymer. Thus, it is considered a promising material that can be used in numerous applications [11-13]. However, although cellulose has a distinctive chemical structure, it is insoluble in the conventional solvent, so it needs modifications to improve its properties and extend the range of its uses [14-16]. 2,2,6,6-tetramethylpiperidine-1-oxyl (TEMPO)

*Corresponding author e-mail: sawsannrc2012@yahoo.com.

Receive Date: 02 November 2021 , Revise Date: 08 December 2021 , Accept Date: 14 December 2021 DOI: 10.21608/EJCHEM.2021.103848.4808

©2022 National Information and Documentation Center (NIDOC)

oxidation is one of the most common methods for oxidation and modification of cellulose to convert the primary hydroxyl groups ($\text{CH}_2\text{-OH}$) in position (C6) to carboxylic (COOH) groups [17-19].

Subsequently, we investigate a new eco-friendly magnetic powder with simple preparation for fingerprint visualization in this work. Firstly, cellulose was oxidized by TEMPO followed by in situ preparation of magnetite and loading of GO. Finally, the prepared materials were characterized by distinctive instrumental techniques consisting of FTIR, XRD, and SEM analysis and detection of latent fingerprint.

2. Materials and Methods

2.1. Materials

Bleached bagasse pulp was supplied from Quena Company of Paper Industry, Egypt, with chemical composition, cellulose (96%), hemicellulose (3%), and lignin (3%). Sodium meta-periodate (NaIO_4), NaBr and 2,2,6,6-tetramethylpiperidine-1-oxyl (TEMPO) were purchased from Sigma Aldrich. Graphite (G) powder (99.9%) was provided by Fisher Scientific UK. Potassium permanganate (>99%) and hydrogen peroxide (30%) were bought from Bio Basic Canada Inc. and Carl Roth GmbH, respectively. Iron (II) sulphate heptahydrate ($\text{FeSO}_4 \cdot 7\text{H}_2\text{O}$) and iron (III) chloride hexahydrate ($\text{FeCl}_3 \cdot 6\text{H}_2\text{O}$) were purchased from S.D. Fine-Chem Ltd. All chemicals and reagents were in analytical grade and used without any purification required before use.

2.2. Oxidation of cellulose

The bleached cellulose pulp was oxidized to carboxy cellulose using by TEMPO oxidation process. Typically, 5 g cellulose was dispersed in 500 mL distilled water, 0.08 g (0.5 mmol) of TEMPO reagent, and 0.8 g (8 mmol) sodium bromide was added, followed by 50 mL (10%) of sodium hypochlorite solution with stirring and adjusting the pH to 10. At the end of the reaction, the pH has been adjusted to a neutral and the product was centrifuged at 7000 rpm. The centrifugation process was repeated using water many times, and finally, the dialysis for 1 week against water was used to complete the purification process [17].

2.3. Preparation of graphene oxide (GO)

Graphite was oxidized to graphene oxide (GO) using the modified Hummer method. A mixture of sulfuric and phosphoric acids (27 mL) in a ratio of 9:1 was stirred for several minutes. A graphite powder (0.225 g) was added into the mixture under stirring, followed

by slowly added potassium permanganate (1.32 g), and continued stirring for another 6h until the solution became dark green. Next, 0.675 mL of hydrogen peroxide was added to eliminate the excess of KMnO_4 and stirred for 10 minutes, then let it cool down. The product GO was washed with 10mL hydrochloric acid with 30 mL deionized water using centrifugation at 5000 rpm for 7 minutes. The supernatant was decanted away, and the residuals were rewashed with $\text{HCl}/\text{H}_2\text{O}$ 3 times. The washed GO was dried at 90 °C in an oven for 24h giving GO powder form [9, 10].

2.4. Preparation of composite

The magnetic oxidized cellulose composite loaded with GO was prepared by in-situ magnetite, followed by the blending technique. First, to the aqueous dispersed oxidized cellulose solution, a mixture of iron (II) and (III) salts (1 and 1.5 g respectively) were added at 30 °C with adjusting the pH to ≈ 10 and stirring for 30 min following by increasing the temperature to 80 °C for another 30 min with continues stirring. Finally, 0.2g of GO was added, and the formed black product of magnetic oxidized cellulose loaded with GO composite (Ox. cellulose/ Fe_3O_4 /GO) was washed with water and dried at 50°C in an oven [20].

2.5. Characterizations

FT-IR spectra were recorded in the range of 400–4000 cm^{-1} on (Shimadzu 8400S) FT-IR Spectrophotometer. The XRD patterns were investigated on a Diano X-ray diffractometer using $\text{Cu K}\alpha$ radiation source energized at 45 kV and a Philips X-ray diffractometer (PW 1930 generator, PW 1820 goniometer) with CuK radiation source ($\lambda=0.15418$ nm), at a diffraction angle range of 2θ from 5 to 80° in reflection mode. The surface morphology was analyzed using Scanning electron microscopy (SEM) FEI IN SPECTS Company, Philips, Holland, environmental scanning without coating. The prepared composite's elemental content was detected by connecting the energy-dispersive X-ray analysis to a scanning electron microscope (TEAM-EDXA). The transmission electron microscope (TEM) using JEOL 1230 (Tokyo, Japan) with an acceleration voltage of 100 KV was also used to study the morphology of oxidized cellulose. The thermal stability was carried out using a TGA Perkin-Elmer (STA6000), with a heating rate (10°C/min) from room temperature to 900 °C under air atmosphere.

2.6. Cytotoxic effect

Cell viability was assessed by the mitochondrial-dependent reduction of yellow MTT (3-(4,5-dimethylthiazol-2-yl)-2,5-diphenyl tetrazolium bromide) to purple formazan (Mosmann 1983). The following procedures were done in a sterile area using

a Laminar flow cabinet biosafety class II level (Baker, SG403INT, Sanford, ME, USA). Cells were suspended in DMEM-F12 medium, 1% antibiotic-antimycotic mixture (10,000 U/mL Potassium Penicillin, 10,000 µg/mL Streptomycin Sulfate and 25 µg/mL Amphotericin B) and 1% L-glutamine at 37 °C under 5% CO₂. Cells were batch cultured for 10 days, then seeded at a concentration of 10 X10³ cells/well in fresh complete growth medium in 96-well microtiter plastic plates at 37 °C for 24 h under 5% CO₂ using a water-jacketed carbon dioxide incubator (Sheldon, TC2323, Cornelius, OR, USA). Media was aspirated, fresh medium (without serum) was added, and cells were incubated either alone (negative control) or with different concentrations of sample to give a final concentration of (100-50-25-12.5-6.25-3.125-0.78 and 1.56 µg/mL). After 48 h of incubation, the medium was aspirated, 40 µl MTT salt (2.5 µg/mL) were added to each well and incubated for a further 4 h at 37 °C under 5% CO₂. To stop the reaction and dissolve the formed crystals, 200 µL of 10 % sodium dodecyl sulphate (SDS) in deionized water was added to each well and incubated overnight at 37°C. DOX was used as a positive control at 100 µg/ml gives 100 % lethality under the same conditions. The absorbance was then measured using a microplate multi-well reader (Bio-Rad Laboratories Inc., model 3350, Hercules, California, USA) at 595 nm and a reference wavelength of 620 nm. A statistical significance was tested between samples and negative control (cells with the vehicle) using an independent t-test by SPSS 11 program. DMSO is the vehicle used to dissolve plant extracts, and its final concentration on the cells was less than 0.2 %. The percentage of change in viability was calculated according to the formula [21].

$$\text{Change in viability (\%)} = \frac{\text{Reading of extract}}{\text{Reading of negative control}} \times 100$$

2.7. Detection of latent fingerprints

The latent fingerprints (LFPs) were collected by gently pressing the clean hands of the same volunteer on the surfaces of the material at room temperature. Next, the synthesized magnetic composite was stained cautiously using a smooth brush with removing the surplus powder by gentle smooth motion until LFPs were enhanced. Finally, the enhanced fingerprints were photographed using a digital camera [8].

3. Results and discussion

3.1. Preparation of graphene oxide (GO)

GO was synthesized by the modified Hummer oxidation method. Through this method, multi-layers

of graphite converted to mono-layer with new groups such as carbonyl, carboxylic, and hydroxyl incorporated in GO matrix. FT-IR spectra of GO (**Figure 1A**) illustrate a band at 3500 cm⁻¹ that was assigned to stretching vibration of the O–H confirming the presence of OH and/or COOH groups within the structure. The band at 2900 cm⁻¹ was due to the C–H bond's symmetric and asymmetric stretching vibration. Also, stretching vibration of carbonyl C=O and/ or C=C appears at 1650 cm⁻¹ [22]. The peak at 2250 cm⁻¹ represents the CO₂ due to the porosity and hygroscopic nature of graphite and a small peak at 650 cm⁻¹ is attributed to OH out-of-plane bending. [23]. This confirmed the presence of various oxygen-containing functional groups like hydroxyl, carboxyl, carbonyl, and epoxy within the GO structure. In addition to FTIR spectra, the X-ray pattern confirmed the formation of GO from graphite which has a distinctive peak at 2θ= 26°, while GO has a characteristic peak at 2θ= 10° due to new groups formation [9, 24]. The peak observed at 44.4° was attributed to reflections from the aluminum holder used [25, 26].

TEM and HR-TEM measurement were also carried out to study the morphology and microstructure of the graphene oxide. As shown in Figure 1c continuous sponge-like architecture with a connected porous texture is clearly observed.

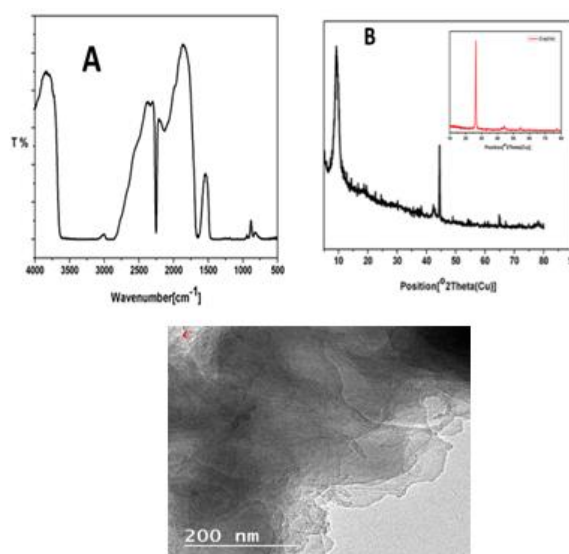


Figure.1. FT-IR spectra of GO (A), XRD pattern of graphite and GO (B), and TEM image of GO (C).

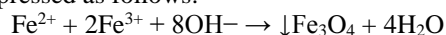
3.2. Oxidation of cellulose

Cellulose was oxidized via TEMPO oxidation that makes oxidation selectively on primary CH₂-OH in position C6 and converts hydroxyl group (OH) to the carboxyl group (COOH). As a result, the reactivity of

cellulose increases and can be modified to another form. The oxidation was confirmed by comparing the FTIR and X-ray spectra of oxidized cellulose with non-oxidized cellulose. **Figure 2B** illustrates the FTIR spectra of cellulose and oxidized cellulose. In cellulose spectra, all the characteristic peaks appear clearly, such as a broad peak at around 3500 cm^{-1} attributed to the stretching vibration of OH groups, the peak at 2900 cm^{-1} of C-H stretching, and the peak at 1632 cm^{-1} which is attributed to OH bending of adsorbed water. The peak at 1048 cm^{-1} is attributed to the stretching vibration of C-O-C ether linkage [27-29]. In oxidized cellulose spectra, the peaks of O-H, C-H, C-O-C, and C=O of the carbonyl group became small due to the degradation process.

3.3. Preparation of oxidized cellulose/Fe₃O₄/GO composite (ox. cellulose/Fe₃O₄/GO)

The magnetite (Fe₃O₄) was incorporated into the cellulose chain by in situ preparation to form a black magnetic product that enhances the easy use by brush. Magnetite particles (Fe₃O₄) were prepared by coprecipitation of ferrous and ferric cations, reaction can be expressed as follows:



At the end of the reaction, GO was added to enhance the performance and visualization of latent fingerprints (**Figure 2A**). As in the case of composite spectra, a new peak appears at 550 cm^{-1} of the Fe₃O₄ [20] and a new peak at 1550 cm^{-1} which is attributed to the presence of GO. As well as the peaks of OH and CH at 3500 and 2900 cm^{-1} expanded due to GO.

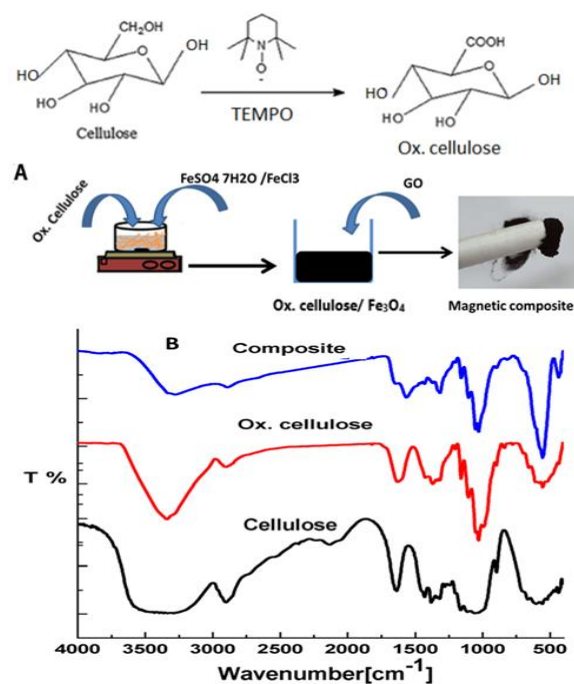


Figure 2. A) magnetic composite formation and B) FTIR of cellulose, ox.cellulose, and magnetic composite.

3.4. Characterizations

3.4.1. Morphology studies

The surface morphology of cellulose, ox.cellulose and ox.cellulose/Fe₃O₄/GO magnetic powder were observed by scanning electron microscopy (SEM) and transmission electron microscopy (TEM). As shown in **Figure 3a**, cellulose has a micro-sized fibrous structure. By TEMPO oxidation of cellulose, the fibrous structure was still in the microstructure but with high distribution with a diameter in the range of $0.03\text{ }\mu\text{m}$ [30].

(**Figure 3b**). The morphological structure of ox.cellulose/Fe₃O₄/GO was studied by SEM also. The surface morphology of the prepared composite have a rougher surface due to the immobilization of magnetite, which aggregates in the form of clusters on the surface of cellulosic fibers (**Figure 3c**). The analysis revealed that the diameters are in the range of micro-sized structure ($10\text{ }\mu\text{m}$) (**Figure 3c**).

Different analytical methods can be used to explore the elemental content of the material; one of these is the EDAX technique used to detect other elements at minimal total ranges. The elemental contents noted from the EDAX analysis confirmed the loaded magnetite onto the composite (**Figure 3d**).

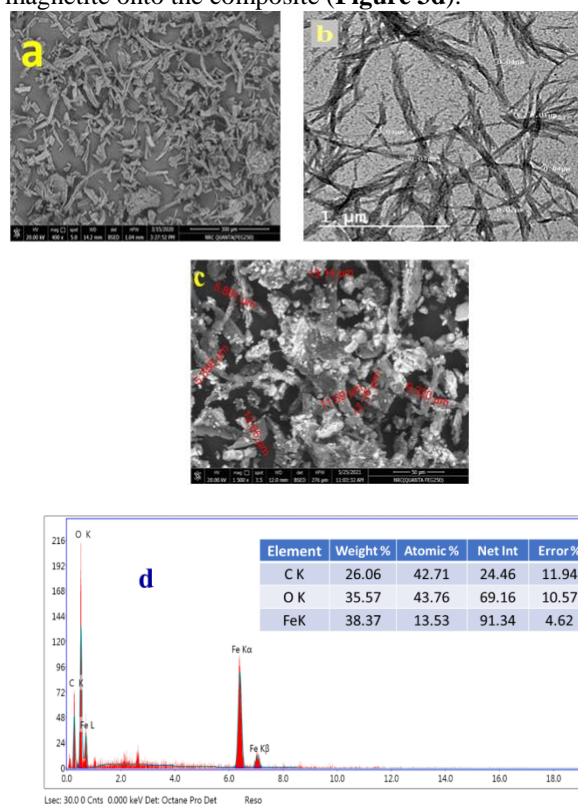


Figure 3. SEM image of cellulose (a), TEM image of oxidized cellulose (b), TEM image of ox. cellulose/Fe₃O₄/GO (c), and EDAX analysis of ox. cellulose/Fe₃O₄/GO composite (d).

3.4.2. X-Ray Diffraction

Figure 4 displays the effect of incorporating Fe₃O₄ and GO onto oxidized cellulose. The cellulose pattern shows two overlapped peaks at $2\theta = 15$ and 16.5° and one sharp peak at $2\theta = 22^\circ$, representing cellulose I less crystalline material [31, 32]. After the oxidation process, the sharp peak at $2\theta = 22^\circ$ broadened, and the two overlapped peaks slightly appeared. In the X-Ray spectra of ox.cellulose/Fe₃O₄/GO composite, the peak of cellulose and the characteristic peak of GO were completely disappeared, and new peaks at $2\theta = 35$ and 45° have appeared that confirmed the loading of Fe₃O₄ onto the surface of the composite.[33, 34].

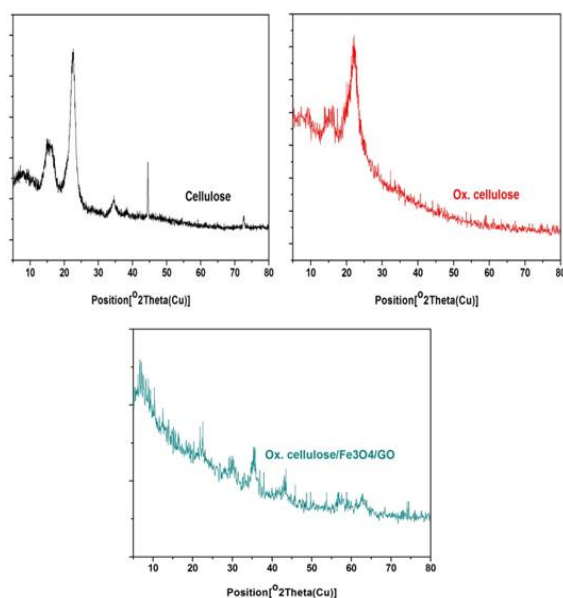


Figure 4. XRD pattern of cellulose, oxidized cellulose, and Ox.cellulose/Fe₃O₄/GO composite.

3.4.3. Thermogravimetric analysis (TGA)

Figure 5 illustrates the thermal stability of oxidized cellulose and magnetic composite where cellulose shows moderate thermal stability. Cellulose degradation occurs through two steps; the first one moisture content losses at 100°C , after those the major content losses at $250\text{--}350^\circ\text{C}$ due to chain decomposition. TGA curve of magnetic composite has illustrated two decomposition stages including the first decomposition at 100°C with weight losses 5%. The early first decomposition temperature may be attributed to low crystallinity of the composite as shown in XRD (Figure 4) compared to cellulose with higher crystallinity leading to higher first stage decomposition temperature. The second decomposition stage involved the thermal degradation

of the main cellulosic skeleton above 320°C . As it seems the thermal stability of composite is higher than cellulose due to presence of GO and Fe₃O₄ that increase thermal stability[20].

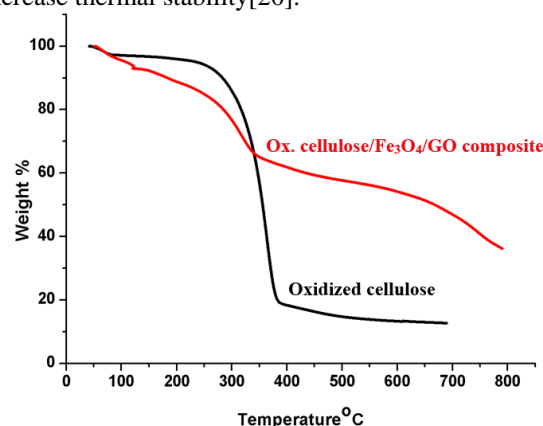


Figure 5. TGA of oxidized cellulose and Ox.cellulose/Fe₃O₄/GO composite.

3.5. Cytotoxic effect

Using the prepared composite in LFP should be non-toxic; therefore its cytotoxicity was evaluated in vitro on human normal immortalized skin fibroblast cells (BJ1). MTT assay is a standard method for determining the cytotoxicity, cell proliferation, and viability of materials. Therefore, the in vitro cytotoxicity was assessed via examining human normal immortalized skin fibroblast cells (BJ1) growth on the prepared composite. The results clarify that the prepared composite can be used for fingerprint detection with high safety profile and high biocompatibility characteristics with human cells (Table 1).

Table 1. MTT assay evaluated human BJ1 fibroblast viability and proliferation after incubation with magnetic composite.

Sample Code	IC ₅₀ (µg/ml)	IC ₉₀ (µg/ml)	Remarks
Magnetic composite	---	---	21.3% at 100ppm
DMSO	---	---	1% at 100ppm
Negative control	---	---	0 %

IC₅₀ and IC₉₀: Lethal concentration of the sample causes the death of 50 and 90% of cells in 48h, respectively.

3.6. Latent fingerprint detection

Synthesized magnetic powder of ox.cellulose/Fe₃O₄/GO was used as fingerprint visualization to develop LFP images. **Figure 6** shows

the LFP image, which was obtained by using a digital mobile camera. This technique depends on the adhesion of composite powder with moisture and/or oily components present on the skin. Due to the size and shape of the fingerprint can be affected by the amount of adhesion of the powders, the removing step must be careful. Thus, magnetic fingerprint powder resolved this problem; the results showed no toxic effect of the prepared composite.

Furthermore, the easy use of magnetic fingerprint powders makes it more comfortable during usage. You need to touch the fingerprint ridges and the excess powders removed with the help of a magnetic brush. Thereby, the magnetic powders are considered safe and reliable for fingerprint experts. This investigation mainly employs iron-based composite for its application in LFPs detection [8, 35]. **Figure 6a&b** shows the LFP images developed by the prepared magnetic powder on smooth non infiltrating Teflon and glass surfaces under normal light. It was evident that the ridge minutiae ridge patterns were identified without any color hindrance under normal light.

Consequently, the prepared magnetic powder such as the ox.cellulose/Fe₃O₄/GO can be used as functional labeling material to identify LFPs. **Figure 6c&d** shows the digital photographs of LFPs stained by an ox. cellulose/Fe₃O₄/GO on the plastic sheet. It was clear that the fingerprints display a well-resolved ridge flow and pattern configuration with an apparent resolution between the bright ridge and dark substrates.

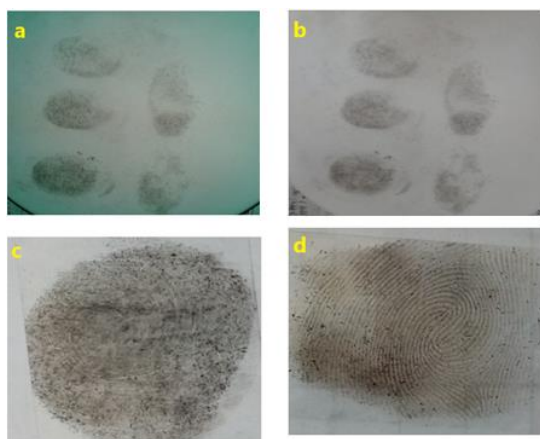


Figure 6. The images of fingerprints using ox.cellulose/Fe₃O₄/GO composite.

Conclusion

The oxidized cellulose/Fe₃O₄/GO composite was successfully developed from in situ syntheses of magnetite in the presence of TEMPO-oxidized cellulose followed by loading GO onto the magnetite oxidized cellulose. The generated composite and its components were characterized, and the results

confirmed the success oxidation of graphite and loading of GO. Furthermore, the non-toxicity of this composite encourages its application as latent fingerprints.

Acknowledgments

The authors would like to acknowledge the financial support for this research from the National Research Centre and Academy of Scientific Research and Technology (ASRT), Egypt, through the Egypt-Hungarian Scientific and Technological Cooperation Program.

Conflicts of Interest

The authors declare no conflict of interest.

References

1. Milenkovic, I., et al., *Fingerprint imaging using N-doped carbon dots*. Carbon, 2019. **144**: p. 791-797.
2. Isenor, D.K. and S.G. Zaky, *Fingerprint identification using graph matching*. Pattern Recognition, 1986. **19**(2): p. 113-122.
3. Bebis, G., T. Deaconu, and M. Georgiopoulos. *Fingerprint identification using Delaunay triangulation*. in *Proceedings 1999 International Conference on Information Intelligence and Systems (Cat. No.PR00446)*. 1999.
4. Zhang, M., et al., *Application of electrodepositing graphene nanosheets for latent fingerprint enhancement*. Electroanalysis, 2014. **26**(1): p. 209-215.
5. Jones, N., et al., *Vacuum metal deposition: developing latent fingerprints on polyethylene substrates after the deposition of excess gold*. Forensic science international, 2001. **123**(1): p. 5-12.
6. Williams, G., H.N. McMurray, and D.A. Worsley, *Latent fingerprint detection using a scanning Kelvin microprobe*. Journal of Forensic Science, 2001. **46**(5): p. 1085-1092.
7. Crane, N.J., et al., *Infrared spectroscopic imaging for noninvasive detection of latent fingerprints*. Journal of forensic sciences, 2007. **52**(1): p. 48-53.
8. Amrutha, V., et al., *Enhanced Sunlight driven photocatalytic performance and visualization of latent fingerprint by green mediated ZnFe₂O₄-RGO nanocomposite*. Arabian Journal of Chemistry, 2020. **13**(1): p. 1449-1465.
9. Dacrory, S., *Antimicrobial Activity, DFT Calculations, and Molecular Docking of Dialdehyde Cellulose/Graphene Oxide Film Against Covid-19*. Journal of Polymers and the Environment, 2021: p. 1-13.
10. Ghanem, A.F. and M.H. Abdel Rehim, *Assisted tip sonication approach for graphene synthesis in aqueous dispersion*. Biomedicines, 2018. **6**(2): p. 63.

11. Dacrory, S., et al., *Development of biodegradable semiconducting foam based on micro-fibrillated cellulose/Cu-NPs*. International journal of biological macromolecules, 2019. **132**: p. 351-359.
12. Mekheimer, R.A., et al., *Green, three component highly efficient synthesis of 2-amino-5, 6, 7, 8-tetrahydro-4-H-chromen-3-carbonitriles in water at ambient temperature*. Green Chemistry Letters and Reviews, 2010. **3**(3): p. 161-163.
13. Abou-Yousef, H., et al., *Biocompatible hydrogel based on aldehyde-functionalized cellulose and chitosan for potential control drug release*. Sustainable Chemistry and Pharmacy, 2021. **21**: p. 100419.
14. Dacrory, S., et al., *Antimicrobial cellulosic hydrogel from olive oil industrial residue*. International journal of biological macromolecules, 2018. **117**: p. 179-188.
15. Dacrory, S., et al., *Functionalization and Cross-Linking of Carboxymethyl Cellulose in Aqueous Media*. Cellulose Chemistry and Technology, 2019. **53** (1-2), : p. 23-33.
16. Mekheimer, R.A., et al., *Simple, three-component, highly efficient green synthesis of thiazolo [3, 2-a] pyridine derivatives under neat conditions*. Synthetic Communications, 2011. **41**(17): p. 2511-2516.
17. Abou-Zeid, R.E., et al., *Novel method of preparation of tricarboxylic cellulose nanofiber for efficient removal of heavy metal ions from aqueous solution*. International journal of biological macromolecules, 2018. **119**: p. 207-214.
18. Kamala, K.H., et al., *Adsorption of Fe ions by modified carrageenan beads with tricarboxy cellulose: kinetics study and four isotherm models*. DESALINATION AND WATER TREATMENT, 2019. **165**: p. 281-289.
19. Toro, R.G., et al., *Study of the effect of titanium dioxide hydrosol on the photocatalytic and mechanical properties of paper sheets*. Materials, 2020. **13**(6): p. 1326.
20. Dacrory, S., et al., *In Situ Synthesis of Fe₃O₄@ Cyanoethyl Cellulose Composite as Antimicrobial and Semiconducting Film*. Carbohydrate Polymers, 2020: p. 116032.
21. Hashem, A.H., et al., *A New Approach for Antimicrobial and Antiviral Activities of Biocompatible Nanocomposite Based on Cellulose, Amino Acid and Graphene Oxide*. Colloids and Surfaces B: Biointerfaces, 2021: p. 112172.
22. Manoratne, C., S. Rosa, and I. Kottegoda, *XRD-HTA, UV visible, FTIR and SEM interpretation of reduced graphene oxide synthesized from high purity vein graphite*. Material Science Research India, 2017. **14**(1): p. 19-30.
23. Faniyi, I., et al., *The comparative analyses of reduced graphene oxide (RGO) prepared via green, mild and chemical approaches*. SN Applied Sciences, 2019. **1**(10): p. 1-7.
24. Ghanem, A.F., et al., *Synergistic effect of zinc oxide nanorods on the photocatalytic performance and the biological activity of graphene nano sheets*. Heliyon, 2020. **6**(2): p. e03283.
25. Dacrory, S., et al., *Cyanoethyl cellulose/BaTiO₃/GO flexible films with electroconductive properties*. ECS Journal of Solid State Science and Technology, 2021. **10**(8): p. 083004.
26. Dacrory, S., *Development of mesoporous foam based on dicarboxylic cellulose and graphene oxide for potential oil/water separation*. Polymer Bulletin, 2021: p. 1-12.
27. Khattab, T.A., et al., *Development of microporous cellulose-based smart xerogel reversible sensor via freeze drying for naked-eye detection of ammonia gas*. Carbohydrate polymers, 2019: p. 196-203.
28. Khattab, T.A., et al., *Smart microfibrillated cellulose as swab sponge-like aerogel for real-time colorimetric naked-eye sweat monitoring*. Talanta, 2019. **205**: p. 120166.
29. Caschera, D., et al., *Green approach for the fabrication of silver-oxidized cellulose nanocomposite with antibacterial properties*. Cellulose, 2020. **27**(14): p. 8059-8073.
30. Adel, A.M., et al., *Chitosan/nanocrystalline cellulose biocomposites based on date palm (Phoenix dactylifera L.) sheath fibers*. Journal of Renewable Materials, 2019. **7**(6): p. 567-582.
31. Liu, C., et al., *Cellulose nanofibers from rapidly microwave-delignified energy cane bagasse and their application in drilling fluids as rheology and filtration modifiers*. Industrial Crops and Products, 2020. **150**: p. 112378.
32. Han, J., et al., *Self-assembling behavior of cellulose nanoparticles during freeze-drying: effect of suspension concentration, particle size, crystal structure, and surface charge*. Biomacromolecules, 2013. **14**(5): p. 1529-1540.
33. Dacrory, S. and A.M. Fahim, *Synthesis, Anti-proliferative activity, Computational studies of tetrazole cellulose utilizing different homogenous catalyst*. Carbohydrate Polymers, 2020: p. 115537.
34. Marnani, N.N. and A. Shabbazi, *A novel environmental-friendly nanobiocomposite synthesis by EDTA and chitosan functionalized magnetic graphene oxide for high removal of Rhodamine B: adsorption mechanism and separation property*. Chemosphere, 2019. **218**: p. 715-725.
35. Choi, M.J., et al., *Fluorescent TiO₂ powders prepared using a new perylene diimide dye: Applications in latent fingerprint detection*.

Forensic science international, 2007. **173**(2-3): p.
154-160.